Published in IET Microwaves, Antennas & Propagation
Received on 17th December 2007
doi: 10.1049/iet-map:20080246

In Special Issue on Asia Pacific Microwave Conference 2007

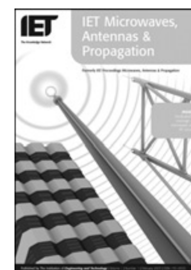

ISSN 1751-8725

Nonlinear and fully distributed field effect transistor modelling procedure using time-domain method

K. Afrooz[1] *A. Abdipour*[1] *A. Tavakoli*[1] *M. Movahhedi*[2]

[1]*Microwave/mm-Wave & Wireless Communication Research Lab, Radio Communication Center of Excellence, Electrical Engineering Department, Amirkabir University of Technology, 424 Hafez Ave., Tehran, Iran*
[2]*Electrical Engineering Department, Shahid Bahonar University of Kerman, Kerman, Iran*
E-mail: kambiz.afrooz@aut.ac.ir

Abstract: An accurate and efficient modelling approach for field effect transistors (FET) as nonlinear active transmission lines is presented. The nonlinear active multiconductor transmission line (NAMTL) equations are obtained by considering the transistor as three active coupled lines operating in a nonlinear regime. This modelling procedure accurately spots the effect of wave propagation along the device electrodes. This modelling approach is applied to an FET by solving the NAMTL equations using a finite-difference time-domain technique. The results of this model are compared with the semi-distributed (slice) model. This method produces more accurate results than the slice model, especially at high frequencies.

1 Introduction

The demand for millimetre-wave monolithic microwave integrated circuits (MMICs) has been increasing rapidly because of the need for higher performance and lower cost. Also, the increasing demand of processing and transmitting more information at a faster rate leads the analogue and digital electronic systems to operate at higher frequencies or higher clock speeds [1]. Therefore the MMICs circuits are used in more and more high-frequency applications. A field effect transistor (FET) is one of the most important devices used in developing MMICs for systems such as an automobile radar and wireless local area network, which operate at high frequencies. To design the MMICs precisely, an accurate FET model is indispensable. As the operating frequency of a microwave FET increases to the millimetre-wave range, the dimensions of the electrodes become comparable with the wavelength, λ_g [2]. When the device width becomes comparable with the wavelength, the reactance of the gate electrode (input active transmission line) becomes different from the drain electrode (output active transmission line) [3]. Thus, the electrodes of the device exhibit different phase velocities for input and output signals. By increasing the frequency or device dimension, the phase cancellation because of the mismatching of the phase velocities will affect the overall performance of the device, especially in the nonlinear regime. In a nonlinear circuit, such as an oscillator, mixer, high-power amplifier, frequency multiplier and so on, several harmonics of the excitation source will be generated in the circuit. Hence, the effect of wave propagation along the device electrodes has a more significant influence on the circuit performance as compared with a linear circuit. In such cases, for accurate modelling, the wave propagation effect needs to be considered in the device modelling. The full-wave analysis and global modelling approach can be used to consider the wave propagation effects along the device structure accurately. However, the computation cost of this type of approach is very expensive [4]. Although, some efficient numerical methods have been recently proposed for reduction in simulation time [5–10], these approaches seem to need more attention to be appropriate for implementing in simulation softwares. On the other hand, device behaviour at high frequencies can be well

© The Institution of Engineering and Technology 2008

Authorized licensed use limited to: University of Waterloo. Downloaded on December 26, 2008 at 00:35 from IEEE Xplore. Restrictions apply.

described using a semi-distributed (slice) model that can be easily implemented in computer aided design (CAD) routines of simulators. In semi-distributed modelling, with the assumption of a quasi transverse electromagnetic (TEM) approximation, the device is divided into finite cascade cells. Each cell contains the coupled electrode transmission lines, resistance and internal inductance of the electrodes, and an intrinsic FET equivalent circuit [2, 11, 12]. The semi-distributed model with both linear and nonlinear lumped elements for the active part has been investigated in several papers. Abdipour and Pacaud [2] applied the semi-distributed model to the FET in a linear regime based on a three-line structure and confirmed the results with measurement data. Also, Ongareau *et al.* [11] considered a semi-distributed model to analyse a FET in a nonlinear regime with the assumption of a two-line structure based on a harmonic balance technique. By increasing the frequency, the semi-distributed model cannot precisely model the wave propagation effect and phase cancellation phenomena on the electrical performance. Therefore to achieve more accurate results in high-frequency applications one needs to develop the semi-distributed model. A fully distributed model is a modified version of the semi-distributed model, in which the number of slices goes to infinity. Thus, the fully distributed model can consider the effect of wave propagation along the device electrodes more accurately than the semi-distributed model although the CPU time of this model is a little greater than the slice model. In this modelling approach, the (TEM) wave propagation is inspected on the electrodes of the device. A fully distributed model of an FET with three active coupled lines in a linear regime is embodied in the active multiconductor transmission lines (AMTL) equation [13]. The AMTL equations are coupled, linear and first-order differential equations that can give a good prediction of FET behaviour in linear and high-frequency applications [13]. These equations are based on the three active coupled lines and, hence, the distributed effect of the source electrode is considered at the AMTL equations for accurate modelling of devices in high-frequency applications [14].

The transistor at the AMTL equation is assumed to operate at the linear region, whereas many microwave circuits such as mixers, power amplifiers and so on operate under nonlinear conditions. Thus, in this paper, we introduce a nonlinear active multiconductor transmission line (NAMTL) equation using the fully distributed model by considering the distributed effect of the source electrode. To obtain these equations, first, the device width is divided into infinity segments. Each segment is considered as a system with a combination of three coupled lines and a conventional equivalent circuit of a FET in the nonlinear regime. The intrinsic FET equivalent circuit in a nonlinear regime modelled on the Curtice cubic model [15]. The Curtice cubic model parameters are obtained from DC and low-frequency measurements. The transmission line theory is applied to a segment of the transistor to obtain the wave equation in a FET structure. Now, this system of nonlinear differential equations (NAMTL equation) must be solved. Since an analytical solution does not exist for this system, this problem is to be solved using a numerical technique. The finite-difference time-domain (FDTD) method is widely used in solving various kinds of electromagnetic problems, wherein lossy, nonlinear, inhomogeneous media and transient problems can be considered [16]. The FDTD technique is used to solve the NAMTL equations. The results achieved from this model (fully distributed) are compared with the slice model at several bias points. It is shown, at the low frequencies, the results of the semi-distributed and fully distributed models are the same. However, by increasing the frequency, the results of two models are not in a good agreement. The fully distributed model is a modified version of the semi-distributed model, when the number of slices increases to the infinity and consider the wave propagation effects. We expect the proposed method becomes more accurate than the slice model.

2 Derivation of the NAMTL equations

Fig. 1 shows a typical millimetre-wave FET. The device consists of three coupled electrodes fabricated on a thin layer of GaAs supported by a semi-insulated GaAs substrate. By increasing the frequency, the dimensions of the device become comparable with the wavelength. In this condition, the distributed effect on the device electrodes should be considered in the device modelling. At a low enough frequency or for a device with dimensions much smaller than the wavelength, the magnitude of longitudinal electromagnetic field is negligible compared with that of the transverse field. Hence, in these cases, the quasi-TEM mode, which is a dominant mode propagated along the device electrode, can be approximated. The fully distributed model is one of the accurate models applied to consider the distributed and wave propagation effects on device behaviour. Thus, the quasi-TEM approximation can be considered and the NAMTL equations are generalised using a fully distributed modelling approach.

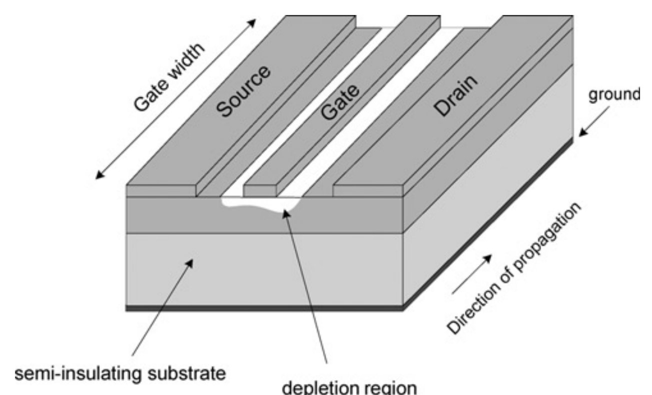

Figure 1 *Schematic showing the structure of a typical millimetre-wave FET*

doi: 10.1049/iet-map:20080246
© The Institution of Engineering and Technology 2008

Authorized licensed use limited to: University of Waterloo. Downloaded on December 26, 2008 at 00:35 from IEEE Xplore. Restrictions apply.

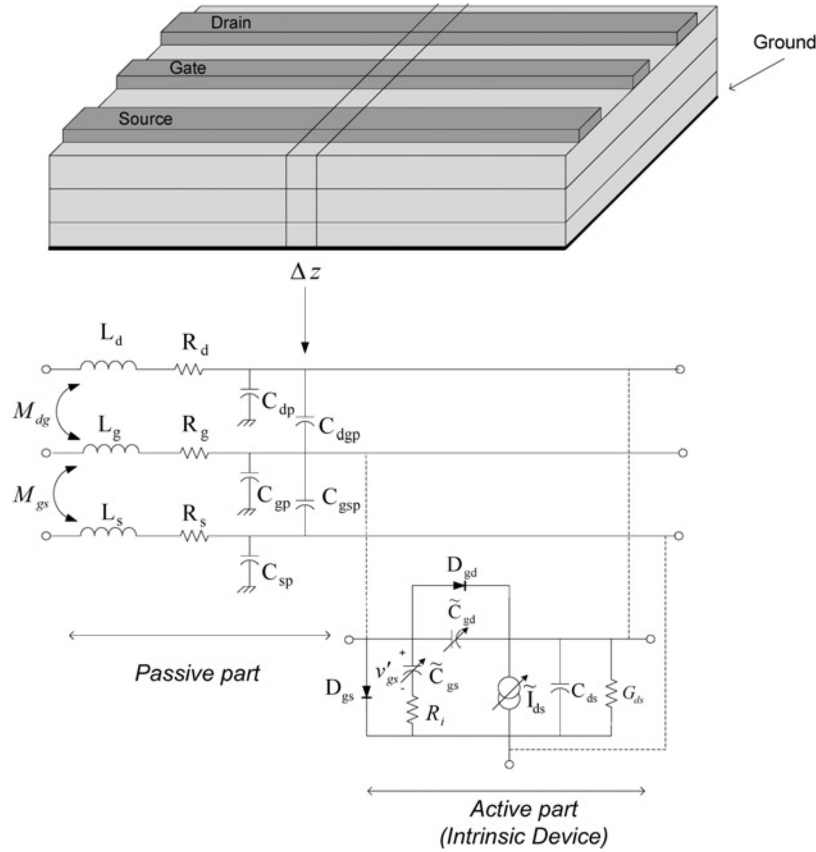

Figure 2 *Different parts of a differential slice in the fully distributed model*

We plan to extract a set of equations that show the transistor's behaviour. A differential section of the device is shown in Fig. 2. Each differential section combines a passive part and an active one. The passive and active parts describe the electromagnetic interaction between the coupled lines and the behaviour of the intrinsic device in the nonlinear regime, respectively. All parameters are per unit length. By applying Kirchhoff's current law to the left loop of the circuit shown in Fig. 2 and by considering the limiting case $\Delta z \rightarrow 0$, we obtain the following three equations

$$\frac{\partial}{\partial z} I_{\mathrm{d}}(z,t) + \tilde{C}_1 \frac{\partial}{\partial t} V_{\mathrm{d}}(z,t) - \tilde{C}_{12} \frac{\partial}{\partial t} V_{\mathrm{g}}(z,t) - C_{13} \frac{\partial}{\partial t} V_{\mathrm{s}}(z,t) + G_{\mathrm{ds}}(V_{\mathrm{d}}(z,t) - V_{\mathrm{s}}(z,t)) + \tilde{I}_{\mathrm{ds}} = 0 \quad (1)$$

$$\frac{\partial}{\partial z} I_{\mathrm{g}}(z,t) - \tilde{C}_{12} \frac{\partial}{\partial t} V_{\mathrm{d}}(z,t) + \tilde{C}_2 \frac{\partial}{\partial t} V_{\mathrm{g}}(z,t) - C_{23} \frac{\partial}{\partial t} V_{\mathrm{s}}(z,t) + \tilde{C}_{\mathrm{gs}} \frac{\partial}{\partial t} \acute{V}_{\mathrm{g}}(z,t) = 0 \quad (2)$$

$$\frac{\partial}{\partial z} I_{\mathrm{s}}(z,t) - C_{13} \frac{\partial}{\partial t} V_{\mathrm{d}}(z,t) - C_{23} \frac{\partial}{\partial t} V_{\mathrm{g}}(z,t) + C_3 \frac{\partial}{\partial t} V_{\mathrm{s}}(z,t) - \tilde{C}_{\mathrm{gs}} \frac{\partial}{\partial t} \acute{V}_{\mathrm{g}}(z,t) - G_{\mathrm{ds}}(V_{\mathrm{d}}(z,t) - V_{\mathrm{s}}(z,t)) - \tilde{I}_{\mathrm{ds}} = 0 \quad (3)$$

where

$$\tilde{C}_1 = C_{\mathrm{d}p} + C_{\mathrm{ds}} + C_{\mathrm{ds}p} + \tilde{C}_{\mathrm{gd}} + C_{\mathrm{gd}p}$$

$$\tilde{C}_2 = C_{\mathrm{g}p} + C_{\mathrm{gs}p} + \tilde{C}_{\mathrm{gd}} + C_{\mathrm{gd}p}$$

$$C_3 = C_{\mathrm{s}p} + C_{\mathrm{ds}} + C_{\mathrm{ds}p} + C_{\mathrm{gs}p}$$

$$\tilde{C}_{12} = \tilde{C}_{\mathrm{gd}} + C_{\mathrm{dg}p}, \quad C_{13} = C_{\mathrm{ds}} + C_{\mathrm{ds}p}, \quad C_{23} = C_{\mathrm{gs}p}$$

Similarly, by applying Kirchhoff's voltage law to the main node of the circuit and considering the limiting case as $\Delta z \rightarrow 0$ in Fig. 2 gives

$$\frac{\partial}{\partial z} V_{\mathrm{d}}(z,t) + R_{\mathrm{d}} I_{\mathrm{d}}(z,t) + L_{\mathrm{d}} \frac{\partial}{\partial t} V_{\mathrm{d}}(z,t) + M_{\mathrm{dg}} \frac{\partial}{\partial t} V_{\mathrm{g}}(z,t) + M_{\mathrm{ds}} \frac{\partial}{\partial t} V_{\mathrm{s}}(z,t) = 0 \quad (4)$$

$$\frac{\partial}{\partial z} V_{\mathrm{g}}(z,t) + R_{\mathrm{g}} I_{\mathrm{g}}(z,t) + L_{\mathrm{g}} \frac{\partial}{\partial t} V_{\mathrm{g}}(z,t) + M_{\mathrm{dg}} \frac{\partial}{\partial t} V_{\mathrm{d}}(z,t) + M_{\mathrm{gs}} \frac{\partial}{\partial t} V_{\mathrm{s}}(z,t) = 0 \quad (5)$$

$$\frac{\partial}{\partial z} V_{\mathrm{s}}(z,t) + R_{\mathrm{s}} I_{\mathrm{s}}(z,t) + L_{\mathrm{s}} \frac{\partial}{\partial t} V_{\mathrm{s}}(z,t) + M_{\mathrm{ds}} \frac{\partial}{\partial t} V_{\mathrm{d}}(z,t) + M_{\mathrm{gs}} \frac{\partial}{\partial t} V_{\mathrm{g}}(z,t) = 0 \quad (6)$$

© The Institution of Engineering and Technology 2008
doi: 10.1049/iet-map:20080246

Authorized licensed use limited to: University of Waterloo. Downloaded on December 26, 2008 at 00:35 from IEEE Xplore. Restrictions apply.

We can also write another equation as follows

$$\acute{V}_g(z,t) + V_s(z,t) + R_i\tilde{C}_{gs}\frac{\partial}{\partial t}\acute{V}_g(z,t) - V_g(z,t) = 0 \quad (7)$$

The Curtice cubic nonlinear model is selected to model the active part (intrinsic device) [15]. In this model, the drain–source current ($\tilde{I}_{ds}$), gate–source junction ($\tilde{Q}_{gs}$) and gate–drain junction ($\tilde{Q}_{gd}$) are rewritten as the following

$$\tilde{I}_{ds} = I_{dso}\tanh(\gamma V_{ds}) \quad (8)$$

with

$$I_{dso} = A_o + A_1V_1 + A_2V_1^2 + A_3V_1^3 + \frac{V_{ds} - V_{dsc}}{R_{dso}} \quad (9)$$

where

$$V_1 = \begin{cases} V_{gs}[1 + \beta(V_{dso} - V_{ds})] & V_{ds} > 0\ \mathrm{V} \\ V_{gd}[1 + \beta(V_{dso} + V_{ds})] & V_{ds} < 0\ \mathrm{V} \end{cases} \quad (10)$$

For values of V_1 below the internally computed maximum pinch-off voltage (V_{pmax}), $\tilde{I}_{ds}$ is replaced with the following expression

$$I_{dso} = A_o + A_1V_{pmax} + A_2V_{pmax}^2 + A_3V_{pmax}^3 + \frac{V_{ds} - V_{dsc}}{R_{dso}} \quad (11)$$

if the value of I_{dso} for $V_{ds} > 0$ V is negative, the drain–source current becomes set to zero. The drain–source and gate–drain charge and capacitance are formulated in the Curtice cubic as follows

$$Q_{gk} = \begin{cases} 2V_{bi}C_{gko}\left[1 - \sqrt{1 - \frac{V_{gk}}{V_{bi}}}\right], & V_{gk} < F_cV_{bi} \\ 2V_{bi}C_{gko}[1 - \sqrt{1 - F_c}] + \left[\left(\frac{C_{gko}}{(1 - F_c)^{3/2}}\right)\left(1 - \frac{3F_c}{2}\right) \times (V_{gk} - F_cV_{bi})\left(\frac{V_{gk}^2 - (F_cV_{bi})^2}{4V_{bi}}\right)\right], & V_{gk} > F_cV_{bi} \end{cases} \quad (12)$$

and

$$C_{gk} = \frac{\partial Q_{gk}}{\partial V_{gk}} = \begin{cases} \frac{C_{gko}}{\sqrt{1 - (V_{gk}/V_{bi})}}, & V_{gk} < F_cV_{bi} \\ \frac{C_{gko}}{(1 - F_c)^{3/2}} \times \left[1 - \frac{3F_c}{2} + \frac{V_{gk}}{2V_{bi}}\right], & V_{gk} > F_cV_{bi} \end{cases} \quad (13)$$

where $k = d, c$, $C_{gco} = C_{gso}$ and $V_{gc} = \acute{V}_{gs}$. Also, C_{gso} and C_{gdo} are the zero-bias gate and drain capacitances, respectively, γ the current saturation, β a coefficient for a pinch-off change with respect to V_{ds}, F_c the forward-bias depletion capacitance coefficient (diode model) and V_{bi} the built-in gate potential.

It is obvious that the value of each element in each segment is per unit length. Hence, some of the Curtice cubic parameters should be converted to per unit parameters.

Equations (1)–(3) and (4)–(7) can be simplified into two matrix equations as the following

$$\frac{\partial}{\partial z}\begin{pmatrix} I_d \\ I_g \\ I_s \\ 0 \end{pmatrix} + \frac{\partial}{\partial t}\begin{pmatrix} \tilde{C}_1 & -\tilde{C}_{12} & -C_{13} & 0 \\ -\tilde{C}_{12} & \tilde{C}_2 & -C_{23} & \tilde{C}_{gs} \\ -C_{13} & -C_{23} & C_3 & -\tilde{C}_{gs} \\ 0 & 0 & 0 & R_i\tilde{C}_{gs} \end{pmatrix}\begin{pmatrix} V_d \\ V_g \\ V_s \\ \acute{V}_g \end{pmatrix} + \begin{pmatrix} G_{ds} & 0 & -G_{ds} & 0 \\ 0 & 0 & 0 & 0 \\ -G_{ds} & 0 & G_{ds} & 0 \\ 0 & -1 & 1 & 1 \end{pmatrix}\begin{pmatrix} V_d \\ V_g \\ V_s \\ \acute{V}_g \end{pmatrix} + \begin{pmatrix} \tilde{I}_{ds} \\ 0 \\ -\tilde{I}_{ds} \\ 0 \end{pmatrix} = 0 \quad (14)$$

$$\frac{\partial}{\partial z}\begin{pmatrix} V_d \\ V_g \\ V_s \end{pmatrix} + \frac{\partial}{\partial t}\begin{pmatrix} L_d & M_{dg} & M_{ds} \\ M_{dg} & L_g & M_{gs} \\ M_{ds} & M_{gs} & L_s \end{pmatrix}\begin{pmatrix} I_d \\ I_g \\ I_s \end{pmatrix} + \begin{pmatrix} R_d & 0 & 0 \\ 0 & R_g & 0 \\ 0 & 0 & R_s \end{pmatrix}\begin{pmatrix} I_d \\ I_g \\ I_s \end{pmatrix} = 0 \quad (15)$$

where I_d, V_d, I_g, V_g and I_s, V_s are the drain, gate and source currents and voltages, respectively; $\acute{V}_g$ is the gate–source capacitance voltage; and I_{ds} is the drain–source current.

3 FDTD solution of the NAMTL equations

The nonlinear fully distributed model of an FET is embodied in the following NAMTL equations

$$\frac{\partial}{\partial z}\acute{\boldsymbol{I}}(z,t) + \tilde{\boldsymbol{C}}(V_d, V_g, V_s, \acute{V}_g)\frac{\partial}{\partial t}\acute{\boldsymbol{V}}(z,t) + \boldsymbol{G}\acute{\boldsymbol{V}}(z,t) + \tilde{\boldsymbol{I}}_{NL}(V_d, V_g, V_s) = 0 \quad (16)$$

$$\frac{\partial}{\partial z}\boldsymbol{V}(z,t) + \boldsymbol{L}\frac{\partial}{\partial t}\boldsymbol{I}(z,t) + \boldsymbol{R}\boldsymbol{I}(z,t) = 0 \quad (17)$$

© The Institution of Engineering and Technology 2008

Authorized licensed use limited to: University of Waterloo. Downloaded on December 26, 2008 at 00:35 from IEEE Xplore. Restrictions apply.

where

$$\boldsymbol{V}(z,t)=\begin{pmatrix}V_{\mathrm{d}}(z,t)\\V_{\mathrm{g}}(z,t)\\V_{\mathrm{s}}(z,t)\end{pmatrix},\quad \boldsymbol{I}(z,t)=\begin{pmatrix}I_{\mathrm{d}}(z,t)\\I_{\mathrm{g}}(z,t)\\I_{\mathrm{s}}(z,t)\end{pmatrix},$$

$$\tilde{\boldsymbol{I}}_{\mathrm{NL}}(z,t)=\begin{pmatrix}\tilde{I}_{\mathrm{ds}}(z,t)\\0\\-\tilde{I}_{\mathrm{ds}}(z,t)\\0\end{pmatrix},\ \acute{\boldsymbol{V}}(z,t)=\begin{pmatrix}V_{\mathrm{d}}(z,t)\\V_{\mathrm{g}}(z,t)\\V_{\mathrm{s}}(z,t)\\\acute{V}_{g}(z,t)\end{pmatrix}$$

$$\text{and}\quad \acute{\boldsymbol{I}}(z,t)=\begin{pmatrix}I_{\mathrm{d}}(z,t)\\I_{\mathrm{g}}(z,t)\\I_{\mathrm{s}}(z,t)\\0\end{pmatrix}$$

The NAMTL equations are coupled, nonlinear and first-order partial differential equations. A numerical technique is needed to solve the NAMTL equations. One of the best methods, which can be employed to solve the NAMTL equations is the FDTD technique. The FDTD technique seeks to approximate the derivatives with regard to discrete solution points defined by the spatial and temporal cells [17]. An explicit time-space centred finite-difference scheme is chosen to discretise the NAMTL equations [14]. Thus, each voltage and adjacent current solution point is separated by $\Delta z/2$. In addition, the time points are also interlaced, and each voltage time point and adjacent current time point are separated by $\Delta t/2$ as illustrated in Fig. 3. To ensure the stability of the discretisation and the second-order accuracy, we interlace the N_z+1 voltage points, $V_1, V_2, \ldots, V_{N_z}, V_{N_z+1}$, and the N_z current points, $I_1, I_2, \ldots, I_{N_z}$, as shown in Fig. 3 [17–19]. Discretising the derivatives in the NAMTL equations using the proposed algorithm gives

$$\frac{\acute{\boldsymbol{I}}_{k}^{\,n+(1/2)}-\acute{\boldsymbol{I}}_{k-1}^{\,n+(1/2)}}{\Delta z}+\tilde{\boldsymbol{C}}(\acute{\boldsymbol{V}}_{k}^{n+1},\acute{\boldsymbol{V}}_{k}^{n})\frac{\acute{\boldsymbol{V}}_{k}^{n+1}-\acute{\boldsymbol{V}}_{k}^{n}}{\Delta t}+\boldsymbol{G}\frac{\acute{\boldsymbol{V}}_{k}^{n+1}+\acute{\boldsymbol{V}}_{k}^{n}}{2}+\tilde{\acute{\boldsymbol{I}}}_{\mathrm{NL}}(\acute{\boldsymbol{V}}_{k}^{n+1},\acute{\boldsymbol{V}}_{k}^{n})=0 \tag{18}$$

with $k=1,2,\ldots,N_z+1$

$$\frac{\boldsymbol{V}_{k+1}^{n+1}-\boldsymbol{V}_{k}^{n+1}}{\Delta z}+\boldsymbol{L}\frac{\boldsymbol{I}_{k}^{n+(3/2)}-\boldsymbol{I}_{k}^{n+(1/2)}}{\Delta t}+\boldsymbol{R}\frac{\boldsymbol{I}_{k}^{n+(3/2)}+\boldsymbol{I}_{k}^{n+(1/2)}}{2}=0 \tag{19}$$

with $k=1,2,\ldots,N_z$.

We denote $\boldsymbol{V}_i^j\equiv\boldsymbol{V}((i-1)\Delta z,\ j\Delta t)$, $\acute{\boldsymbol{V}}_i^j\equiv\acute{\boldsymbol{V}}((i-1)\Delta z,\ j\Delta t)$, $\boldsymbol{I}_i^j\equiv\boldsymbol{I}((i-1/2)\Delta z, j\Delta t)$, $\acute{\boldsymbol{I}}_i^j\equiv\acute{\boldsymbol{I}}((i-(1/2)\ r\Delta z, j\Delta t)$, $\tilde{\acute{\boldsymbol{I}}}_{\mathrm{NL}}=[\tilde{\acute{I}}_{\mathrm{ds}},0,\ -\tilde{\acute{I}}_{\mathrm{ds}},0]^{\mathrm{T}}$

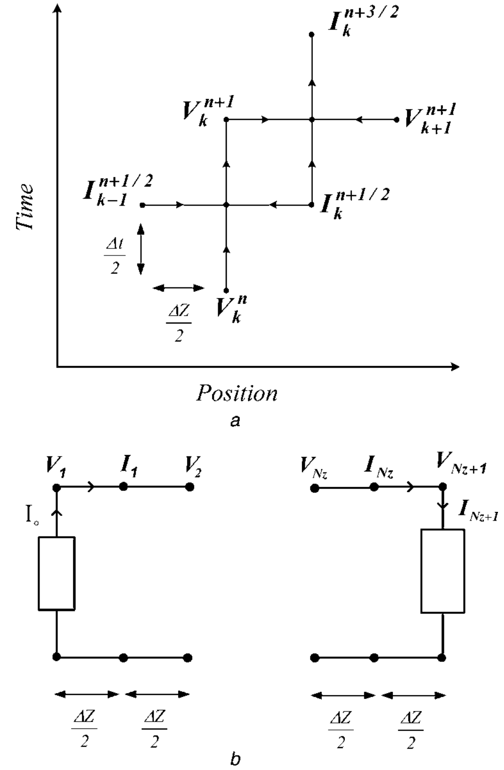

Figure 3 *Relation between the spatial and temporal discretisation and terminal voltages and currents*

a Relation between the spatial and temporal discretisation to achieve second-order accuracy in the discretisation of the derivatives
b Discretisation of the terminal voltages and currents

where

$$\tilde{\acute{I}}_{\mathrm{ds}}=\acute{I}_{\mathrm{ds}o}\tanh\left(\gamma\frac{V_{dk}^{n}+V_{dk}^{n+1}-V_{sk}^{n}-V_{sk}^{n+1}}{2}\right) \tag{20}$$

and

$$\acute{I}_{\mathrm{ds}o}=A_o+A_1\acute{V}_1+A_2\acute{V}_1^2+A_3\acute{V}_1^3+\frac{V_{dk}^{n}+V_{dk}^{n+1}-V_{sk}^{n}-V_{sk}^{n+1}-2V_{\mathrm{ds}c}}{2R_{\mathrm{ds}o}} \tag{21}$$

$$\acute{V}_1=\begin{cases}\dfrac{V_{gk}^{n}+V_{gk}^{n+1}-V_{sk}^{n}-V_{sk}^{n+1}}{2}\times\left[1+\beta\left(V_{\mathrm{ds}o}-\dfrac{V_{dk}^{n}+V_{dk}^{n+1}-V_{sk}^{n}-V_{sk}^{n+1}}{2}\right)\right], & V_{dk}^{n}+V_{dk}^{n+1}>V_{sk}^{n}+V_{sk}^{n+1}\\ \dfrac{V_{gk}^{n}+V_{gk}^{n+1}-V_{dk}^{n}-V_{dk}^{n+1}}{2}\times\left[1+\beta\left(V_{\mathrm{ds}o}+\dfrac{V_{dk}^{n}+V_{dk}^{n+1}-V_{sk}^{n}-V_{sk}^{n+1}}{2}\right)\right], & V_{dk}^{n}+V_{dk}^{n+1}<V_{sk}^{n}+V_{sk}^{n+1}\end{cases} \tag{22}$$

© The Institution of Engineering and Technology 2008
IET Microw. Antennas Propag., 2008, Vol. 2, No. 8, pp. 886–897
doi: 10.1049/iet-map:20080246

Authorized licensed use limited to: University of Waterloo. Downloaded on December 26, 2008 at 00:35 from IEEE Xplore. Restrictions apply.

For values of $\acute{V}_1$ below the internal computed maximum pinch-off voltage (V_{pmax}), $\tilde{\tilde{I}}_{\mathrm{ds}}$ is replaced with the following expression

$$\acute{I}_{\mathrm{ds}o} = A_o + A_1 V_{\mathrm{pmax}} + A_2 V_{\mathrm{pmax}}^2 + A_3 V_{\mathrm{pmax}}^3 + \frac{V_{dk}^n + V_{dk}^{n+1} - V_{sk}^n - V_{sk}^{n+1} - 2V_{\mathrm{dsc}}}{2R_{\mathrm{ds}o}} \quad (23)$$

If the $\acute{I}_{\mathrm{ds}o}$ value for $V_{dk}^n + V_{dk}^{n+1} > V_{sk}^n + V_{sk}^{n+1}$ is negative, the drain–source current becomes set to zero. The drain–source and gate–drain charges and capacitances are modelled in the Curtice cubic model as follows

$$C_{gm} = \begin{cases} \dfrac{C_{gmo}}{\sqrt{1-((V_{gk}^n + V_{gk}^{n+1} - V_{mk}^n - V_{mk}^{n+1})/2V_{bi})}}, & V_{gk}^n + V_{gk}^{n+1} - V_{mk}^n - V_{mk}^{n+1} < 2F_c V_{bi} \\ \dfrac{C_{gmo}}{(1-F_c)^{3/2}}\left[1 - \dfrac{3F_c}{2} + \dfrac{V_{gk}^n + V_{gk}^{n+1} - V_{mk}^n - V_{mk}^{n+1}}{2V_{bi}}\right], & V_{gk}^n + V_{gk}^{n+1} - V_{mk}^n - V_{mk}^{n+1} > 2F_c V_{bi} \end{cases} \quad (24)$$

where $m = d, c$, $C_{\mathrm{gc}o} = C_{\mathrm{gs}o}$ and $\acute{V}_{gsk}^n + \acute{V}_{gsk}^{n+1} = V_{gk}^n + V_{gk}^{n+1} - V_{ck}^n - V_{ck}^{n+1}$.

Simplifying (18) and (19) we obtain

$$\boldsymbol{F}_{\mathrm{NL}}(V_{mk}^{n+1}, V_{mk}^n, \acute{V}_{gk}^{n+1}, \acute{V}_{gk}^n, I_{mk}^{n+(1/2)}) = 0, \quad m = d, s, g \quad (25)$$

$$\boldsymbol{I}_k^{n+(3/2)} = \left(\frac{\boldsymbol{L}}{\Delta t} + \frac{\boldsymbol{R}}{2}\right)^{-1}\left\{\left(\frac{\boldsymbol{L}}{\Delta t} - \frac{\boldsymbol{R}}{2}\right)\boldsymbol{I}_k^{n+(1/2)} - \frac{\boldsymbol{V}_{k+1}^{n+1} - \boldsymbol{V}_k^{n+1}}{\Delta z}\right\} \quad (26)$$

Because of the simplicity and accuracy, the leap-frog algorithm for alternately computing the voltage and the current is used to solve the NAMTL equations [16]. In this algorithm, first, the solutions start with an initially relaxed line having zero voltage and current values. Then, voltages along the electrode of the transistor are solved for a fixed time from (25) in terms of the previous solutions, and then currents are solved from (26) in terms of these and previous values.

3.1 Solution of the nonlinear equation $F_{NL} = 0$

Equation (25) should be solved to calculate the voltage along the electrodes of the transistor. One of the most useful and best known algorithms to solve nonlinear systems of equations is the Newton–Raphson method that converges faster than the bisection and false position methods [20]. Exactly, (25) is a set of four algebraic nonlinear equations with four unknown parameters as the following

$$\boldsymbol{F}_{\mathrm{NL}} = [F_{1\mathrm{NL}}, F_{2\mathrm{NL}}, F_{3\mathrm{NL}}, F_{4\mathrm{NL}}]^{\mathrm{T}} \quad (27)$$

Our purpose is to obtain the four unknown parameters (V_{dk}^{n+1}, V_{gk}^{n+1}, V_{sk}^{n+1}, $\acute{V}_{gk}^{n+1}$). In this technique, first, we start with the initial values for unknown parameters and then the Jacobian matrix is calculated upshot. The value of the unknown parameters are calculated in the next stage as follows

$$(\acute{\boldsymbol{V}}_k^{n+1})^{m+1} = (\acute{\boldsymbol{V}}_k^{n+1})^m - (\boldsymbol{JAC}((\acute{\boldsymbol{V}}_k^{n+1})^m))^{-1} \times \boldsymbol{F}_{\mathrm{NL}}((\acute{\boldsymbol{V}}_k^{n+1})^m) \quad (28)$$

this iterative algorithm is executed until $|\boldsymbol{F}_{\mathrm{NL}}((\boldsymbol{V}_k^{n+1})^m)| < \epsilon$. The Jacobian matrix is given as

$$\boldsymbol{JAC} = \left.\frac{\partial \boldsymbol{F}_{\mathrm{NL}}}{\partial \acute{\boldsymbol{V}}}\right|_{\acute{V}_k^{n+1}} = \begin{pmatrix} \frac{\partial F_{1NL}}{\partial V_{dk}^{n+1}} & \frac{\partial F_{1NL}}{\partial V_{gk}^{n+1}} & \frac{\partial F_{1NL}}{\partial V_{sk}^{n+1}} & \frac{\partial F_{1NL}}{\partial \acute{V}_{gk}^{n+1}} \\ \frac{\partial F_{2NL}}{\partial V_{dk}^{n+1}} & \frac{\partial F_{2NL}}{\partial V_{gk}^{n+1}} & \frac{\partial F_{2NL}}{\partial V_{sk}^{n+1}} & \frac{\partial F_{2NL}}{\partial \acute{V}_{gk}^{n+1}} \\ \frac{\partial F_{3NL}}{\partial V_{dk}^{n+1}} & \frac{\partial F_{3NL}}{\partial V_{gk}^{n+1}} & \frac{\partial F_{3NL}}{\partial V_{sk}^{n+1}} & \frac{\partial F_{3NL}}{\partial \acute{V}_{gk}^{n+1}} \\ \frac{\partial F_{4NL}}{\partial V_{dk}^{n+1}} & \frac{\partial F_{4NL}}{\partial V_{gk}^{n+1}} & \frac{\partial F_{4NL}}{\partial V_{sk}^{n+1}} & \frac{\partial F_{4NL}}{\partial \acute{V}_{gk}^{n+1}} \end{pmatrix} \quad (29)$$

This procedure gives us the voltages along the electrodes of the transistor. Also, the voltage of the gate–source capacitance is obtained. Then, using the voltage at the new time step we can obtain the current at the new step using (26).

4 Boundary conditions

In many applications, in microwave circuits, transistors are used in the common source configuration because of high stability and high gain of this configuration. In this configuration, the source electrode is grounded at the beginning and at the end of electrode. Also, the transistors have been excited at the beginning of the gate electrode and loaded at the end of drain electrode for the consideration of the wave effects [3–8]. Thus, we need to investigate this case of loading and exciting configuration, whereas the other configuration can be simply investigated using the NAMTL equations. Fig. 4 shows the assumed structure of the transistor with the biasing and loading circuits. With this consideration of biasing circuits, (1), (2) and (7) for $z = 0$ and $z = W$ become

© The Institution of Engineering and Technology 2008

Authorized licensed use limited to: University of Waterloo. Downloaded on December 26, 2008 at 00:35 from IEEE Xplore. Restrictions apply.

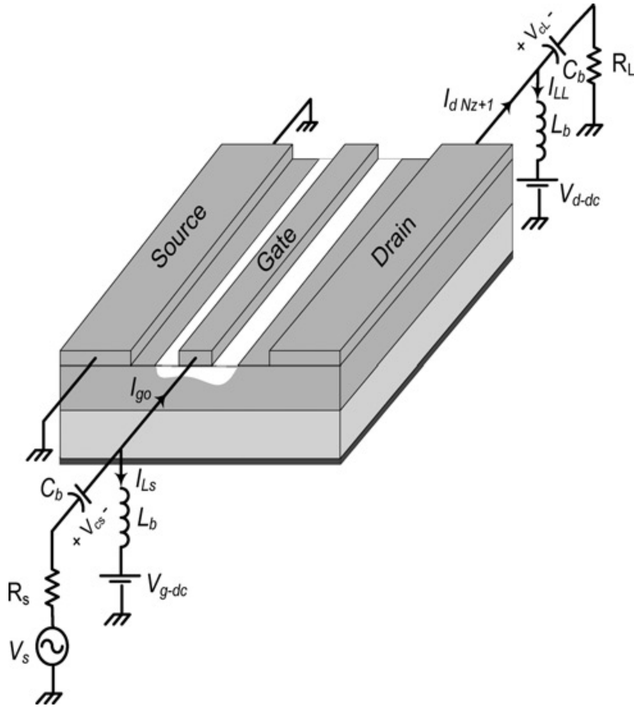

Figure 4 *Biasing and loading circuits considered for the transistor*

$(V_s(z, t) = 0|_{z=0,z=W})$, respectively

$$\frac{\partial}{\partial z} I_d(z, t) + \tilde{C}_1 \frac{\partial}{\partial t} V_d(z, t) - \tilde{C}_{12} \frac{\partial}{\partial t} V_g(z, t) + G_{ds} V_d(z, t) + \tilde{I}_{ds} = 0|_{z=0,z=W} \quad (30)$$

$$\frac{\partial}{\partial z} I_g(z, t) - \tilde{C}_{12} \frac{\partial}{\partial t} V_d(z, t) + \tilde{C}_2 \frac{\partial}{\partial t} V_g(z, t) + \tilde{C}_{gs} \frac{\partial}{\partial t} \acute{V}_g(z, t) = 0|_{z=0,z=W} \quad (31)$$

$$V_g(\acute{z}, t) + R_i \tilde{C}_{gs} \frac{\partial}{\partial t} \acute{V}_g(z, t) - V_g(z, t) = 0|_{z=0,z=W} \quad (32)$$

Also, two equations are given as KVL and KCL in the biasing circuit at the beginning of the gate electrode as follows (Fig. 4)

$$-V_{in}(t) + R_s C_b \frac{\partial V_{cs}(t)}{\partial t} + V_{cs}(t) + V_g(0, t) = 0 \quad (33)$$

$$-V_{g-dc} - L_b \frac{\partial I_{Ls}(t)}{\partial t} + V_g(0, t) = 0 \quad (34)$$

Equations (30)–(34) can be simplified as

$$\boldsymbol{F1}_{NL} = \frac{\partial \acute{\boldsymbol{I}}(z, t)}{\partial z} + \acute{\boldsymbol{C}} \frac{\partial}{\partial t} \boldsymbol{X}(z, t) + \acute{\boldsymbol{G}} \boldsymbol{X}(z, t) + \tilde{\acute{\boldsymbol{I}}}_{NL} + \boldsymbol{V}_{in}(t) = 0|_{z=0} \quad (35)$$

where

$$\acute{\boldsymbol{I}}(z, t) = \begin{pmatrix} I_d(z, t) \\ I_g(z, t) \\ 0 \\ 0 \\ 0 \end{pmatrix}, \quad \boldsymbol{X}(z, t) = \begin{pmatrix} V_d(z, t) \\ V_g(z, t) \\ \acute{V}_g(z, t) \\ V_{cs}(t) \\ I_{Ls}(t) \end{pmatrix},$$

$$\acute{\boldsymbol{I}}_{NL} = \begin{pmatrix} \tilde{I}_{ds}(z, t) \\ 0 \\ 0 \\ 0 \\ 0 \end{pmatrix}, \quad \boldsymbol{V}_{in}(t) = \begin{pmatrix} 0 \\ 0 \\ 0 \\ -V_{in}(t) \\ -V_{g-dc} \end{pmatrix},$$

$$\acute{\boldsymbol{G}} = \begin{pmatrix} G_{ds} & 0 & 0 & 0 & 0 \\ 0 & 0 & 0 & 0 & 0 \\ 0 & -1 & 1 & 0 & 0 \\ 0 & 1 & 0 & 1 & 0 \\ 0 & 1 & 0 & 0 & 0 \end{pmatrix}$$

$$\acute{\boldsymbol{C}} = \begin{pmatrix} \tilde{C}_1 & -\tilde{C}_{12} & 0 & 0 & 0 \\ -\tilde{C}_{12} & \tilde{C}_2 & \tilde{C}_{gs} & 0 & 0 \\ 0 & 0 & R_i \tilde{C}_{gs} & 0 & 0 \\ 0 & 0 & 0 & R_s C_b & 0 \\ 0 & 0 & 0 & 0 & -L_b \end{pmatrix}$$

Therefore the NAMTL equations at $z = 0$ become (35). Applying the FDTD technique to (35) and considering Fig. 3, (this equation requires that we replace Δz with $\Delta z/2$) gives

$$\boldsymbol{F1}_{NL} = \frac{\acute{\boldsymbol{I}}_1^{n+(1/2)} - \acute{\boldsymbol{I}}_0^{n+(1/2)}}{\Delta z/2} + \acute{\boldsymbol{C}} \frac{\boldsymbol{X}_1^{n+1} - \boldsymbol{X}_1^n}{\Delta t} + \acute{\boldsymbol{G}} \frac{\boldsymbol{X}_1^{n+1} + \boldsymbol{X}_1^n}{2} + \frac{\boldsymbol{V}_{in}^{n+1} + \boldsymbol{V}_{in}^n}{2} + \tilde{\acute{\boldsymbol{I}}}_{NL}(\boldsymbol{X}_1^{n+1}, \boldsymbol{X}_1^n) = 0 \quad (36)$$

where $\acute{\boldsymbol{I}}_0^{n+(1/2)} = [I_{d0}^{n+(1/2)}, I_{g0}^{n+(1/2)}, 0, 0, 0]^T = [0, C_b((V_{cs}^{n+1} - V_{cs}^n)/\Delta t) - ((I_{Ls}^n + I_{Ls}^{n+1})/2), 0, 0, 0]^T$.

Exactly, (36) is a set of five algebraic nonlinear equations with five unknown parameters as the following

$$\boldsymbol{F1}_{NL} = [F1_{1NL}, F1_{2NL}, F1_{3NL}, F1_{4NL}, F1_{5NL}]^T \quad (37)$$

Our purpose is to obtain the five unknown parameters (V_{d1}^{n+1}, V_{g1}^{n+1}, $\acute{V}_{g1}^{n+1}$, V_{cL}^{n+1} and I_{Ls}^{n+1}).

Also, two equations are given as KVL and KCL in the biasing circuit at the end of the drain electrode as follows

$$R_L C_b \frac{\partial V_{cL}(t)}{\partial t} + V_{cL}(t) - V_d(W, t) = 0 \quad (38)$$

$$-V_{d-dc} - L_b \frac{\partial I_{LL}(t)}{\partial t} + V_d(W, t) = 0 \quad (39)$$

© The Institution of Engineering and Technology 2008
doi: 10.1049/iet-map:20080246

Authorized licensed use limited to: University of Waterloo. Downloaded on December 26, 2008 at 00:35 from IEEE Xplore. Restrictions apply.

Equations (30)–(32) and, (38) and (39) can be simplified as

$$\boldsymbol{FL}_{\mathrm{NL}} = \frac{\partial \acute{\tilde{\boldsymbol{I}}}(z,t)}{\partial z} + \acute{\tilde{\tilde{\boldsymbol{C}}}} \frac{\partial}{\partial t}\acute{\boldsymbol{X}}(z,t) + \acute{\tilde{\boldsymbol{G}}}\acute{\boldsymbol{X}}(z,t) + \tilde{\tilde{\boldsymbol{I}}}_{\mathrm{NL}} + \acute{\boldsymbol{V}}_{in}(t) = 0|_{z=W} \tag{40}$$

where

$$\acute{\boldsymbol{X}}(z,t) = \begin{pmatrix} V_{\mathrm{d}}(z,t) \\ V_{\mathrm{g}}(z,t) \\ \acute{V}_{\mathrm{g}}(z,t) \\ V_{cL}(t) \\ I_{LL}(t) \end{pmatrix}, \quad \acute{\boldsymbol{V}}_{\mathrm{in}}(t) = \begin{pmatrix} 0 \\ 0 \\ 0 \\ 0 \\ -V_{d-dc} \end{pmatrix},$$

$$\acute{\tilde{\tilde{\boldsymbol{C}}}} = \begin{pmatrix} \tilde{C}_1 & -\tilde{C}_{12} & 0 & 0 & 0 \\ -\tilde{C}_{12} & \tilde{C}_2 & \tilde{C}_{\mathrm{gs}} & 0 & 0 \\ 0 & 0 & R_i\tilde{C}_{\mathrm{gs}} & 0 & 0 \\ 0 & 0 & 0 & R_L C_b & 0 \\ 0 & 0 & 0 & 0 & -L_b \end{pmatrix}$$

$$\text{and} \quad \acute{\tilde{\boldsymbol{G}}} = \begin{pmatrix} G_{\mathrm{ds}} & 0 & 0 & 0 & 0 \\ 0 & 0 & 0 & 0 & 0 \\ 0 & -1 & 1 & 0 & 0 \\ -1 & 0 & 0 & 1 & 0 \\ 1 & 0 & 0 & 0 & 0 \end{pmatrix}$$

Applying the FDTD technique to (40) and considering Fig. 3, (this equation requires that we replace Δz with $\Delta z/2$), gives

$$\boldsymbol{FL}_{\mathrm{NL}} = \frac{\acute{\tilde{\boldsymbol{I}}}^{n+(1/2)}_{N_z+1} - \acute{\tilde{\boldsymbol{I}}}^{n+(1/2)}_{N_z}}{\Delta z/2} + \acute{\tilde{\tilde{\boldsymbol{C}}}} \frac{\acute{\boldsymbol{X}}^{n+1}_{N_z+1} - \acute{\boldsymbol{X}}^{n}_{N_z+1}}{\Delta t} + \acute{\tilde{\boldsymbol{G}}} \frac{\acute{\boldsymbol{X}}^{n+1}_{N_z+1} + \acute{\boldsymbol{X}}^{n}_{N_z+1}}{2} + \frac{\acute{\boldsymbol{V}}^{n+1}_{\mathrm{in}} + \acute{\boldsymbol{V}}^{n}_{\mathrm{in}}}{2} + \tilde{\tilde{\boldsymbol{I}}}_{\mathrm{NL}}(\acute{\boldsymbol{X}}^{n}_{N_z+1}, \acute{\boldsymbol{X}}^{n+1}_{N_z+1}) = 0 \tag{41}$$

where $\acute{\tilde{\boldsymbol{I}}}^{n+(1/2)}_{N_z+1} = [I^{n+(1/2)}_{dN_z+1}, I^{n+(1/2)}_{gN_z+1}, 0, 0, 0]^{\mathrm{T}} = [C_b(V^{n+1}_{cL} - V^{n}_{cL})/\Delta t) + (I^{n}_{LL} + I^{n+1}_{LL})/2, 0, 0, 0, 0]^{\mathrm{T}}$

Exactly, (41) is a set of five algebraic nonlinear equations with five unknown parameters as the following

$$\boldsymbol{FL}_{\mathrm{NL}} = [FL_{1\mathrm{NL}}, FL_{2\mathrm{NL}}, FL_{3\mathrm{NL}}, FL_{4\mathrm{NL}}, FL_{5\mathrm{NL}}]^{\mathrm{T}} \tag{42}$$

Our purpose is to obtain the five unknown parameters ($V^{n+1}_{dN_z+1}$, $V^{n+1}_{gN_z+1}$, $\acute{V}^{n+1}_{gN_z+1}$, V^{n+1}_{cL} and I^{n+1}_{LL}).

Thus, the finite difference approximation of the NAMTL equations can be written as follows

For $k = 1$

$$(\boldsymbol{X}^{n+1}_1)^{m+1} = (\boldsymbol{X}^{n+1}_1)^{m} - (\boldsymbol{JAC}_1((\boldsymbol{X}^{n+1}_1)^{m}))^{-1} \times \boldsymbol{F1}_{\mathrm{NL}}((\boldsymbol{X}^{n+1}_1)^{m}) \tag{43}$$

where

$$\boldsymbol{X}^{n+1}_1 = [V^{n+1}_{d1}, V^{n+1}_{g1}, \acute{V}^{n+1}_{g1}, V^{n+1}_{cs}, I^{n+1}_{Ls}]^{\mathrm{T}} \tag{44}$$

and

$$\boldsymbol{JAC}_1 = \frac{\partial \boldsymbol{F1}_{\mathrm{NL}}}{\partial \boldsymbol{X}_1}\bigg|_{X^{n+1}_1} = \begin{pmatrix} \frac{\partial F_{1NL}}{\partial V^{n+1}_{d1}} & \frac{\partial F_{1NL}}{\partial V^{n+1}_{g1}} & \frac{\partial F_{1NL}}{\partial \acute{V}^{n+1}_{g1}} & \frac{\partial F_{1NL}}{\partial V^{n+1}_{cs}} & \frac{\partial F_{1NL}}{\partial I^{n+1}_{Ls}} \\ \frac{\partial F_{2NL}}{\partial V^{n+1}_{d1}} & \frac{\partial F_{2NL}}{\partial V^{n+1}_{g1}} & \frac{\partial F_{2NL}}{\partial \acute{V}^{n+1}_{g1}} & \frac{\partial F_{2NL}}{\partial V^{n+1}_{cs}} & \frac{\partial F_{2NL}}{\partial I^{n+1}_{Ls}} \\ \frac{\partial F_{3NL}}{\partial V^{n+1}_{d1}} & \frac{\partial F_{3NL}}{\partial V^{n+1}_{g1}} & \frac{\partial F_{3NL}}{\partial \acute{V}^{n+1}_{g1}} & \frac{\partial F_{3NL}}{\partial V^{n+1}_{cs}} & \frac{\partial F_{3NL}}{\partial I^{n+1}_{Ls}} \\ \frac{\partial F_{4NL}}{\partial V^{n+1}_{d1}} & \frac{\partial F_{4NL}}{\partial V^{n+1}_{g1}} & \frac{\partial F_{4NL}}{\partial \acute{V}^{n+1}_{g1}} & \frac{\partial F_{4NL}}{\partial V^{n+1}_{cs}} & \frac{\partial F_{4NL}}{\partial I^{n+1}_{Ls}} \\ \frac{\partial F_{5NL}}{\partial V^{n+1}_{d1}} & \frac{\partial F_{5NL}}{\partial V^{n+1}_{g1}} & \frac{\partial F_{5NL}}{\partial \acute{V}^{n+1}_{g1}} & \frac{\partial F_{5NL}}{\partial V^{n+1}_{cs}} & \frac{\partial F_{5NL}}{\partial I^{n+1}_{Ls}} \end{pmatrix} \tag{45}$$

For $k = 2, 3, \ldots, Nz$

$$(\acute{\boldsymbol{V}}^{n+1}_k)^{m+1} = (\acute{\boldsymbol{V}}^{n+1}_k)^{m} - (\boldsymbol{JAC}((\acute{\boldsymbol{V}}^{n+1}_k)^{m}))^{-1} \times \boldsymbol{F}_{\mathrm{NL}}((\acute{\boldsymbol{V}}^{n+1}_k)^{m}) \tag{46}$$

where

$$\boldsymbol{JAC} = \frac{\partial \boldsymbol{F}_{\mathrm{NL}}}{\partial \acute{\boldsymbol{V}}}\bigg|_{\acute{V}^{n+1}_k} = \begin{pmatrix} \frac{\partial F_{1NL}}{\partial V^{n+1}_{dk}} & \frac{\partial F_{1NL}}{\partial V^{n+1}_{gk}} & \frac{\partial F_{1NL}}{\partial V^{n+1}_{sk}} & \frac{\partial F_{1NL}}{\partial \acute{V}^{n+1}_{gk}} \\ \frac{\partial F_{2NL}}{\partial V^{n+1}_{dk}} & \frac{\partial F_{2NL}}{\partial V^{n+1}_{gk}} & \frac{\partial F_{2NL}}{\partial V^{n+1}_{sk}} & \frac{\partial F_{2NL}}{\partial \acute{V}^{n+1}_{gk}} \\ \frac{\partial F_{3NL}}{\partial V^{n+1}_{dk}} & \frac{\partial F_{3NL}}{\partial V^{n+1}_{gk}} & \frac{\partial F_{3NL}}{\partial V^{n+1}_{sk}} & \frac{\partial F_{3NL}}{\partial \acute{V}^{n+1}_{gk}} \\ \frac{\partial F_{4NL}}{\partial V^{n+1}_{dk}} & \frac{\partial F_{4NL}}{\partial V^{n+1}_{gk}} & \frac{\partial F_{4NL}}{\partial V^{n+1}_{sk}} & \frac{\partial F_{4NL}}{\partial \acute{V}^{n+1}_{gk}} \end{pmatrix} \tag{47}$$

For $k = N_z + 1$

$$(\acute{\boldsymbol{X}}^{n+1}_{N_z+1})^{m+1} = (\acute{\boldsymbol{X}}^{n+1}_{N_z+1})^{m} - \boldsymbol{JAC}_L((\acute{\boldsymbol{X}}^{n+1}_{N_z+1})^{m})^{-1} \times \boldsymbol{FL}_{\mathrm{NL}}((\acute{\boldsymbol{X}}^{n+1}_{N_z+1})^{m}) \tag{48}$$

© The Institution of Engineering and Technology 2008

Authorized licensed use limited to: University of Waterloo. Downloaded on December 26, 2008 at 00:35 from IEEE Xplore. Restrictions apply.

where

$$\acute{X}_{N_z+1}^{n+1} = [V_{dN_z+1}^{n+1}, V_{gN_z+1}^{n+1}, \acute{V}_{gN_z+1}^{n+1}, V_{cL}^{n+1}, I_{LL}^{n+1}]^{\mathrm{T}} \tag{49}$$

And

$$JAC_L = \frac{\partial FL_{\mathrm{NL}}}{\partial \acute{X}}\bigg|_{\acute{X}_{N_z+1}^{n+1}}$$

$$= \begin{pmatrix} \frac{\partial F_{1NL}}{\partial V_{dN_z+1}^{n+1}} & \frac{\partial F_{1NL}}{\partial V_{gN_z+1}^{n+1}} & \frac{\partial F_{1NL}}{\partial \acute{V}_{gN_z+1}^{n+1}} & \frac{\partial F_{1NL}}{\partial V_{cL}^{n+1}} & \frac{\partial F_{1NL}}{\partial I_{LL}^{n+1}} \\ \frac{\partial F_{2NL}}{\partial V_{dN_z+1}^{n+1}} & \frac{\partial F_{2NL}}{\partial V_{gN_z+1}^{n+1}} & \frac{\partial F_{2NL}}{\partial \acute{V}_{gN_z+1}^{n+1}} & \frac{\partial F_{2NL}}{\partial V_{cL}^{n+1}} & \frac{\partial F_{2NL}}{\partial I_{LL}^{n+1}} \\ \frac{\partial F_{3NL}}{\partial V_{dN_z+1}^{n+1}} & \frac{\partial F_{3NL}}{\partial V_{gN_z+1}^{n+1}} & \frac{\partial F_{3NL}}{\partial \acute{V}_{gN_z+1}^{n+1}} & \frac{\partial F_{3NL}}{\partial V_{cL}^{n+1}} & \frac{\partial F_{3NL}}{\partial I_{LL}^{n+1}} \\ \frac{\partial F_{4NL}}{\partial V_{dN_z+1}^{n+1}} & \frac{\partial F_{4NL}}{\partial V_{gN_z+1}^{n+1}} & \frac{\partial F_{4NL}}{\partial \acute{V}_{gN_z+1}^{n+1}} & \frac{\partial F_{4NL}}{\partial V_{cL}^{n+1}} & \frac{\partial F_{4NL}}{\partial I_{LL}^{n+1}} \\ \frac{\partial F_{5NL}}{\partial V_{dN_z+1}^{n+1}} & \frac{\partial F_{5NL}}{\partial V_{gN_z+1}^{n+1}} & \frac{\partial F_{5NL}}{\partial \acute{V}_{gN_z+1}^{n+1}} & \frac{\partial F_{5NL}}{\partial V_{cL}^{n+1}} & \frac{\partial F_{5NL}}{\partial I_{LL}^{n+1}} \end{pmatrix} \tag{50}$$

and for $k = 2, 3, \ldots, Nz$

$$I_k^{n+(3/2)} = \left(\frac{L}{\Delta t} + \frac{R}{2}\right)^{-1} \left\{ \left(\frac{L}{\Delta t} - \frac{R}{2}\right) I_k^{n+(1/2)} - \frac{V_{k+1}^{n+1} - V_k^{n+1}}{\Delta z} \right\} \tag{51}$$

The voltages and currents are solved by iterating k for a fixed time step and then iterating the time. Fig. 5 shows a flowchart that describes the solution of the problem.

5 Numerical results

Here, the proposed approach is used for modelling a sub-micrometre-gate GaAs transistor. The device has a 0.2 μm × 100 μm gate. The input and output nodes are connected to the beginning and the end of the gate and drain electrodes, respectively. The source electrode is grounded at the beginning and the end of the electrode. The structure of the considered transistor and its biasing and loading circuits are shown in Fig. 4. The values of elements used in the distributed model are shown in Table 1 and parameters of the Curtice cubic model are listed in Table 2. This transistor is simulated at the several bias points using the fully distributed model and its results are compared with the slice model to confirm the results of this study. First, the transistor is biased at $V_{\mathrm{gs}} = 0$ V, $V_{\mathrm{ds}} = 5$ V and the device excited by a 20 GHz sinusoidal excitation source with a 1.5 V amplitude. Figs. 6 and 7 show the voltage and current at the end of drain electrode using the fully distributed and slice models under this bias condition, respectively. As these figures show,

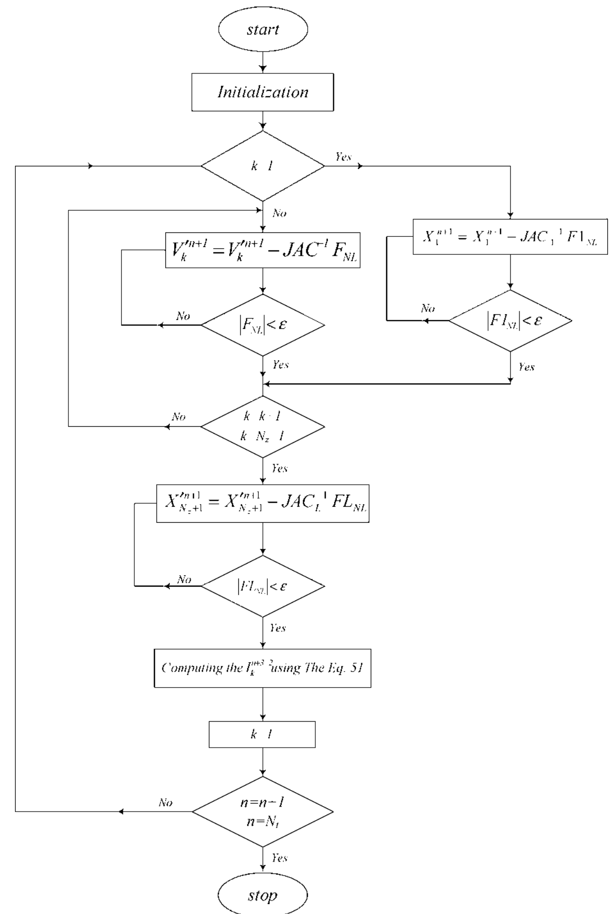

Figure 5 *Flowchart of leap-frog algorithm for solution of the NAMTL equations*

Table 1 Numerical values of the lumped distributed model elements

The distributed model elements	Numerical values (per unit length)
L_d	780 nH/m
L_s	780 nH/m
L_g	161 nH/m
M_{gd}	360 nH/m
M_{gs}	360 nH/m
M_{ds}	240 nH/m
C_{gp}	0.6 pF/m
C_{dp}	87 pF/m
C_{sp}	148 pF/m
C_{gdp}	29 pF/m
C_{gsp}	29 pF/m
C_{dsp}	61 pF/m

© The Institution of Engineering and Technology 2008
doi: 10.1049/iet-map:20080246

Authorized licensed use limited to: University of Waterloo. Downloaded on December 26, 2008 at 00:35 from IEEE Xplore. Restrictions apply.

Table 2 Curtice cubic parameter values

$A_o = 0.058$	$C_{gso} = 0.048216$ pF	$R_{dso} = 273.7828\ \Omega$
$A_1 = 0.1034$	$C_{gdo} = 0.021008$ pF	$A_2 = -0.00924$
$A_3 = -0.048$	$V_{bi} = 0.76$ V	$\beta = 0.021295$
$\gamma = 2.3457$	$V_{dso} = 5$ V	$F_c = 0.5$
$R_i = 0\ \Omega$	$V_{To} = -1.2$ V	$V_{dsc} = 5$ V

there is a good agreement between the fully distributed and slice models. The drain voltage spectrum at the end of the drain electrode is presented in Fig. 8, which describes the nonlinear characteristic of the transistor under this condition very well. The load cycle for this transistor, at $V_{gs} = -0.5$ V, $V_{ds} = 5$ V, excited by a source with a 2 V amplitude and $f = 30$ GHz when the load is a 50 Ω resistance parallel with a 15 fF capacitance, is shown in Fig. 9. The result of the fully distributed model is compared with that of the slice model. Fig. 10 depicts the results of the fully distributed and slice models at $V_{gs} = -0.5$ V, $V_{ds} = 4$ V and with an excitation source with a 2 V amplitude but at a frequency of 60 GHz. In this figure, a fractional difference exists between these two models because of the high-frequency effects. Here, the device dimension becomes comparable with the wavelength. Moreover, the slice model cannot consider the effect of wave propagation along the device electrodes and accurately analyse

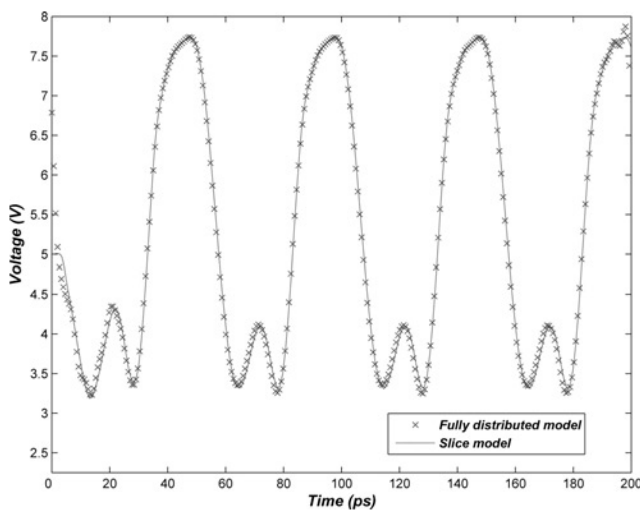

Figure 6 *Voltage at the end of drain electrode when the device is biased at $V_{ds} = 5$ V, $V_{gs} = 0$ V and excited by a 20 GHz sinusoidal excitation source with a 1.5 V amplitude*

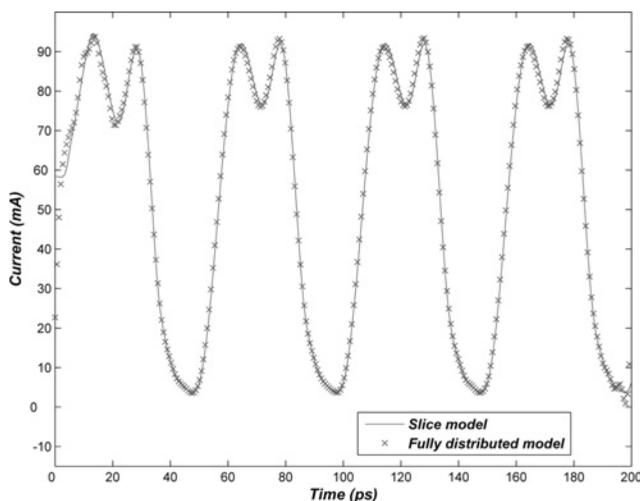

Figure 7 *Current at the end of drain electrode when the device is biased at $V_{ds} = 5$ V, $V_{gs} = 0$ V and excited by a 20 GHz sinusoidal excitation source with 1.5 V amplitude*

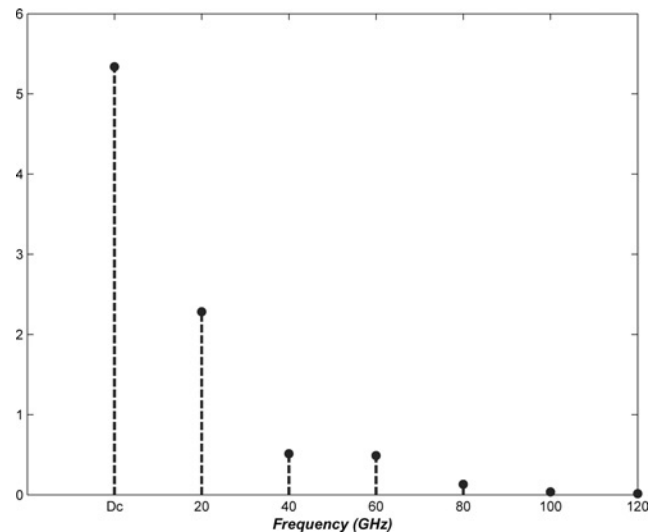

Figure 8 *Drain voltage spectrum at the end of drain electrode when the device is biased at $V_{ds} = 5$ V, $V_{gs} = 0$ V and excited by a 20 GHz sinusoidal excitation source with 1.5 V amplitude*

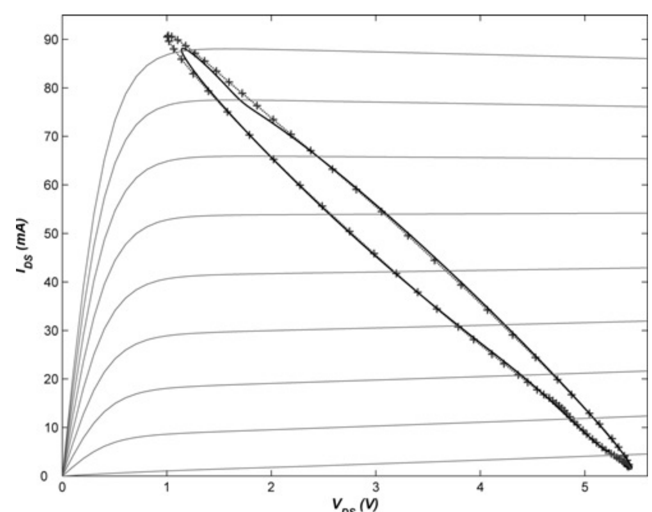

Figure 9 *Load cycle at $V_{ds} = 5$ V and $V_{gs} = -0.5$ V and a source with 2 V amplitude and $f = 30$ GHz when load is a 50 Ω resistance parallel with a 10 fF capacitance*

Fully distributed model (+++) and slice model (−−−)

doi: 10.1049/iet-map:20080246
© The Institution of Engineering and Technology 2008

Authorized licensed use limited to: University of Waterloo. Downloaded on December 26, 2008 at 00:35 from IEEE Xplore. Restrictions apply.

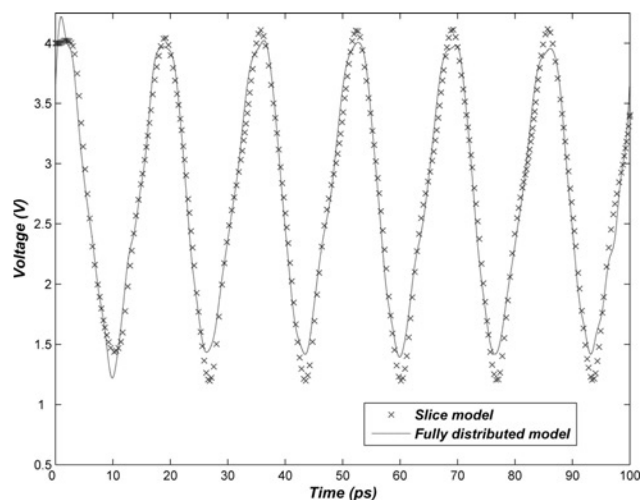

Figure 10 *Voltage at the end of drain electrode when the device is biased at $V_{ds} = 4$ V, $V_{gs} = -0.5$ V having a source with 1.5 V amplitude and $f = 60$ GHz*

it. Since the fully distributed model is a modified version of the slice model when the number of slices becomes infinite, so, the results of this model is more accurate especially at the high-frequency applications. In a nonlinear circuit, because of higher-order harmonics, these effects are more antiseptic than the linear circuits. In most of the papers, the source electrode is assumed grounded at overall the electrode whereas the source electrode is grounded at the beginning and the end. In this work, the distributed effect of the source electrode is considered to obtain accurate results. The voltage at the middle of the source electrode using the fully distributed and slice models when the transistor is biased at $V_{gs} = -0.5$ V, $V_{ds} = 4$ V with a 20 GHz sinusoidal excitation source and a 1.5 V amplitude is shown in Fig. 11. This figure shows that the distributed effect of the source electrode must be accounted for the analysis of high-frequency devices and circuits. Finally, the device being biased at $V_{ds} = 3.5$ V, and $V_{gs} = -1$ V, and the frequency of the

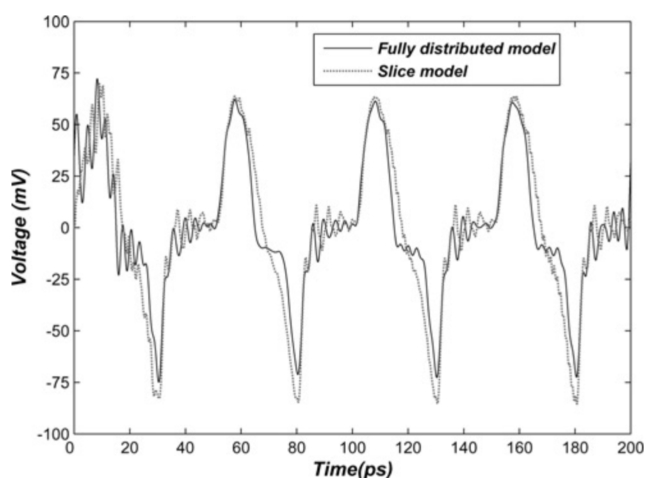

Figure 11 *Voltage at the middle of source electrode at $V_{ds} = 4$ V, $V_{gs} = -0.5$ V and excited by a 20 GHz sinusoidal excitation source with 1.5 V amplitude*

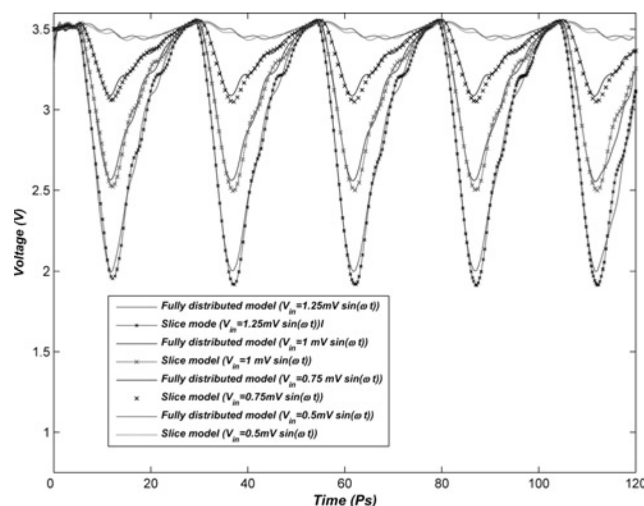

Figure 12 *Voltage at the end of drain electrode when the device is biased at $V_{ds} = 3.5$ V, $V_{gs} = -1$ V and excited by a 40 GHz sinusoidal excitation source with different amplitudes*

excitation source being 40 GHz, the voltages of the end of the drain electrode are plotted in Fig. 12 for the fully distributed and slice models for several amplitudes of the excitation source.

6 Conclusion

The NAMTL equations have been introduced using a fully distributed model based on a three-line structure. These equations can accurately predict the behaviour of microwave/millimetre wave transistors in a nonlinear regime. The FDTD technique is used to solve these nonlinear equations in the time domain. This modelling approach is applied to an FET and the results, for example the voltage and current waveforms are compared with those of the slice model. At a low frequency, the results of the fully distributed model have a good agreement with those of the slice model. However, by increasing the frequency, a fractional difference exists between two models. Since the device dimension is comparable with the wavelength, the wave propagation effects obtained with the fully distributed model are more accurate than those with the slice model. Therefore in high-frequency applications, the use of the fully distributed model is recommended. In addition, in devices with a width comparable to the wavelength, the distributed effect of the source electrode must be considered. Another advantage of this model is the ease of its integration into CAD optimisers.

7 References

[1] IMTIAZ S.M.S., GHAZALY S.M.: 'Global modeling of millimeter-wave circuits: electromagnetic simulation of amplifiers', *IEEE Trans. Microw. Theory Tech.*, 1997, **45**, (12), pp. 2208–2216

[2] ABDIPOUR A., PACAUD A.: 'Complete sliced model of microwave FET's and comparison with lumped model and

© The Institution of Engineering and Technology 2008

doi: 10.1049/iet-map:20080246

Authorized licensed use limited to: University of Waterloo. Downloaded on December 26, 2008 at 00:35 from IEEE Xplore. Restrictions apply.

experimental results', *IEEE Trans. Microw. Theory Tech.*, 1996, **44**, (1), pp. 4–9

[3] GHAZALY S.M., ITOH .T.: 'Traveling-wave inverted-gate field-effect transistor: concept, analysis, and potential', *IEEE Trans. Microw. Theory Tech.*, 1989, **37**, pp. 1027–1032

[4] ALSUNAIDI M.A., IMTIAZ S.M.S., GHAZALY .S.M.: 'Electromagnetic wave effects on microwave transistors using a full-wave time-domain model', *IEEE Trans. Microw. Theory Tech.*, 1996, **44**, pp. 799–808

[5] GHAZALY S.M., ITOH T.: 'Inverted-gate field-effect transistors: novel high frequency structures', *IEEE Trans. Electron. devices*, 1988, **35**, pp. 810–817

[6] GOASGUEN S., TOMEH M., GHAZALY S.M.: 'Electromagnetic and semiconductor device simulation using interpolating wavelets', *IEEE Trans. Microw. Theory Tech.*, 2001, **49**, (12), pp. 2258–2265

[7] HUSSEIN Y.A., EL.GHAZALY S.M.: 'Modeling and optimization of microwave devices and circuits using genetic algorithms', *IEEE Trans. Microw. Theory Tech.*, 2004, **52**, (1), pp. 329–336

[8] MOVAHHEDI M., ABDIPOUR A.: 'Efficient numerical methods for simulation of high-frequency active devics', *IEEE Trans. Microw. Theory Tech.*, 2006, **54**, (6), pp. 2636–2645

[9] MOVAHHEDI M., ABDIPOUR A.: 'Improvement of active microwave device modeling using filter-bank transforms'. Proc. 35th Euro. Microwave, Conf., Paris, France, 2005, pp. 1113–1117

[10] MOVAHHEDI M., ABDIPOUR A.: 'Accelerating the transient simulation of semiconductor devices using filter-bank transforms', *Int. J. Numer. Model*, 2006, **19**, pp. 47–67

[11] ONGAREAU E., BOSISIO R.G., AUBOURG M., OBREGON J., GAYRAL M.: 'A non-linear and distributed modeling procedure of FETs', *Int. J. Numer. Model.*, 1994, **7**, pp. 309–319

[12] WALIULLAH M., GHAZALY S.M., GOODNICK S.: 'Large-signal circuit-based time domain analysis of high frequency devices including distributed effects'. Microwave Symp. Digest, IEEE MTT-S Int., 2002, vol. 3, pp. 2145–2148

[13] AFROOZ K., ABDIPOUR A., TAVAKOLI A., MOVAHHEDI M.: 'Time-domain analysis of active transmission line using FDTD techniques (application to microwave/mm-wave transistors)', *Prog. Electromagn. Res.*, 2007, **PIER 77**, pp. 309–328

[14] AFROOZ K., ABDIPOUR A., TAVAKOLI A., MOVAHHEDI M.: 'FDTD analysis of small signal model for GaAs MESFETs based on three line structure'. Asia-Pacific Microwave Conf. (APMC 2007), Bangkok, Thailand, December 2007

[15] CURTICE W.R., ETTENBERG M.: 'A nonlinear GaAs FET model for use in the design of output circuits for power amplifiers', *IEEE Trans. Microw. Theory Tech.*, 1985, **33**, (12), pp. 1383–1394

[16] TAFLOVE A.: 'Computational electrodynamics the finite-difference time-domain method' (Artech House, Norwood, MA, 1996)

[17] PAUL .C.R.: 'Incorporation of terminal constraints in the FDTD analysis of transmission lines', *IEEE Trans. Electromag. Compat.*, 1994, **36**, pp. 85–91

[18] ORLANDI A., PAUL C.R.: 'FDTD analysis of lossy, multiconductor transmission lines terminated in arbitary loads', *IEEE Trans. Electromagn. Compat.*, 1996, **38**, pp. 388–399

[19] RODEN A.J., PAUL C.R., SMITH W.T., GEDNEY D.S.: 'Finite-difference, time-domain analysis of lossy transmission lines', *IEEE Trans. Electromagn. Compat.*, 1996, **38**, pp. 15–24

[20] YPMA J.T.: 'Historical development of the Newton–Raphson method', *Soc. Ind. Appl. Math.*, 1995, **4**, (1), pp. 531–551

doi: 10.1049/iet-map:20080246
© The Institution of Engineering and Technology 2008

Authorized licensed use limited to: University of Waterloo. Downloaded on December 26, 2008 at 00:35 from IEEE Xplore. Restrictions apply.